Materials Science and Engineering A 527 (2010) 5018–5025

Contents lists available at ScienceDirect

Materials Science and Engineering A

journal homepage: www.elsevier.com/locate/msea

On characterisation of local stress–strain properties in friction stir welded aluminium AA 5083 sheets using micro-tensile specimen testing and instrumented indentation technique

D. Rao, J. Heerens*, G. Alves Pinheiro, J.F. dos Santos, N. Huber

Institute of Materials Research, Materials Mechanics, GKSS Research Centre GmbH, Max-Planck-Straße 1, 21502 Geesthacht, Germany

ARTICLE INFO

Article history:
Received 18 August 2009
Received in revised form 15 April 2010
Accepted 16 April 2010

Keywords:
Stress–strain properties
Weld joints
Hardness
Artificial neural network
Residual stress

ABSTRACT

Stress–strain property variations in welded joints are frequently characterized by determining local stress–strain curves across the joint. A commonly and widely accepted method is testing of micro-tensile specimens where the specimens have to be mechanically extracted form the joint and subsequently tested and analysed similar to that of a conventional tensile tests. A recently developed procedure for the determination of local stress–strain properties is based on instrumented indentation testing where the force–depth curves are analysed via artificial neural networks in order to derive local stress–strain curves. In order to verify this new method on welded joints, this method has been applied to a friction stir weld in 3 mm thick aluminium AA 5083 sheet material. It turned out that the local stress–strain curves derived by instrumented indentation tests and neural networks are compatible with that obtained from micro-tensile testing. Further on, the article gives advises on a proper tests specimen preparation as well as on the treatment of possible residual stresses.

1. Introduction

Mechanical properties provide basic information on the strength of materials as for example needed for designing safe and reliable structures and components. Many properties are typically measured by uniaxial tensile tests. In cases of welded components it is often helpful to measure the Vickers hardness distribution across the weld to estimate the variation of mechanical strength and the degree of under- or overmatching [1] of the weld. Another example of application is optimisation of welding process parameters where hardness measurements are often used to monitor the associated strength variations of the weld joint [2]. Because hardness measurements provide rather qualitative information on the variation of the stress–strain behaviour, other more sophisticated methods have been developed during the last decade. One option is the determination of so called local stress–strain curves derived by testing micro-tensile specimens extracted from the weld joint [3].

Research has also focused at the capability of instrumented indentation test to provide tensile properties from spherical indentation experiments [4–7]. These tests are less destructive, quick to perform, multi-repeatable within the same weld joint and only a relatively small piece of material is required. Some of the proposed procedures are based on optimization methods coupled with elastic–plastic finite-element simulation. For power law hardening models, having only two dimensionless mechanical properties (σ_y/E, n), the inverse problem can be reduced to a unique solution given in form of a polynomial fit to an inverse function derived point wise from finite element simulations [8,9].

In cases where more complex constitutive models are of interest, such as the unified plasticity model of Chaboche, an explicit representation of the desired inverse function determining the material parameters from measured load-depth data can not be derived so easily. Here, artificial neural networks (NN) allow analysing the available information, which is hidden in the finite element results. Huber and Tsakmakis [10] applied a viscoplastic material model for simulating the indentation response of a spherical indenter. Based on that model a well-trained set of artificial neural networks for analysing the experimental force–depth curves was developed [11,12] in order to identify material property data including true stress–strain curve. Meanwhile this NN-method has become commercially available [13] and it has been successfully applied to a number of homogeneous metallic materials [14,15].

Whereas the micro-tensile specimen test technique has become common practice during the last years, little is known about the validity of the NN-method for characterising stress–strain properties in under- or overmatched welded joints. In this case, problems may arise from residual stresses which are usually present in the welded area. Residual stresses do affect the force–depth curves. Because the NN-method is based on stress-free material it cannot

* Corresponding author. Fax: +49 4152 87 2534.
E-mail address: juergen.heerens@gkss.de (J. Heerens).

0921-5093/$ – see front matter © 2010 Elsevier B.V. All rights reserved.
doi:10.1016/j.msea.2010.04.047

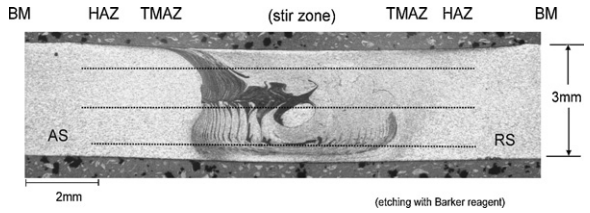

Fig. 1. Macro-structure on sheet crosssection of the FSW-joint. The dotted lines indicate paths where hardness has been measured.

properly account for errors caused by residual stresses. Therefore, there is a high risk that a straight forward application of the NN-method to welded joints will provide invalid results.

One solution for this problem has been recently provided by a new analytical model, which allows to estimate the error in the measured hardness and to correct the force–depth curve for a known residual stress state [16]. This approach can be applied in cases where the residual stress field, i.e. the in-plane residual stress components in the indented region of the weld, is known. In most practical situations this requires additional experimental effort with X-ray or neutron diffraction and in many laboratories the experimental facilities for determining the residual stresses are not available.

A common way of reducing residual stresses from metal surfaces is slotting. It causes a relaxation of the residual stress present in the surface layer which is then ready for performing a valid indentation tests. Associated with such slotting it has to be taken into account that it may also significantly reduce the deformation constraint of the tested volume, which alters the measured force–depth curve. In order to avoid or at least minimise such constraint effect, clear rules regarding a proper surface cutting must be provided.

This paper presents an example where the NN-method is used to characterize the deformation property gradient in an under-matched friction stir joint by determining a set of local stress–strain curves using instrumented indentation tests analysed by neural networks. In order to avoid possible errors due to residual stress the surface of the indentation specimen was mechanically slotted. Numerical simulations were performed to provide practical guidance on a proper specimen surface slotting which avoids an unduly reduction of indentation constraint.

In order to validate the local stress–strain curves derived via the indentation test method, a large set of small micro-tensile specimens extracted from the weld joint have been tested. It was found that instrumented indentation and micro-tensile experiments provide compatible local stress–strain curves. The results demonstrate the validity of the indentation test method for quantifying stress–strain property gradients in friction stir weld joints.

2. Test material, friction stir welded joint and microstructure

The material investigated was a rolled sheet of the alloy AA 5083 (Al–4.5Mg–0.6Mn) with a thickness of 3 mm. This material is widely used in ship building, tank and vehicle construction. Butt joints have been produces by friction stir welding (FSW). The welding was performed using a tool with a shoulder and pin diameter of 5 mm and 12 mm, respectively. The tool speed was 1800 rpm. The welding speed was 1000 mm/min associated with a force of 9.5 kN. These process parameters have been chosen in order to purposely generate an under-matching joint. In this way substantial microstructure changes would be present to validate the experimental methodology proposed in the present study. For more detailed information regarding the process and bonding mechanisms see [17,18].

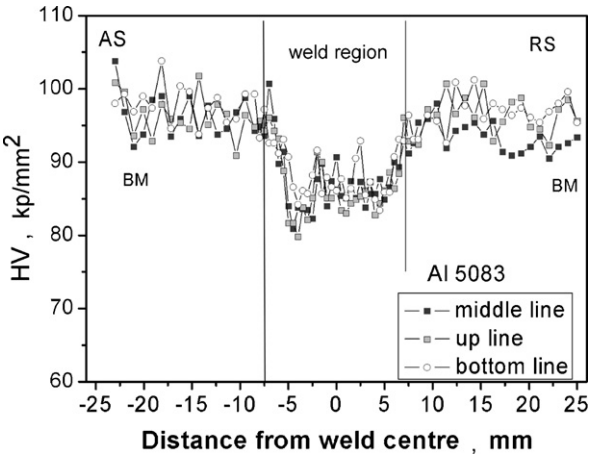

Fig. 2. Vickers hardness measured on the sheet crosssection along the three paths shown in Fig. 1.

Fig. 1 shows the weld macrostructure on the joint crosssection. Besides the base material (BM) it distinguishes between "advancing side" (AS) and "retreating side" (RS). Typical microstructure regions are the stir zone, the thermo mechanical affected zone (TMAZ) and the heat affected zone (HAZ). The ring or layer structure in the centre of the figure is formed by intensive stir which leads to bonding of the two sheets. For a more detailed description of this microstructure see [19].

An overview of the mechanical property variation across a joint can be obtained from conventional Vickers hardness measurements. Fig. 2 shows the hardness distribution on the crosssection of the weld joint. The BM has an average hardness about 95 HV, while the HAZ, TMAZ and stir zone are significantly softer. The hardness profile across the joint seems to be asymmetrically, it decrease more sharply at the AS compared to that of the RS. Moreover, Fig. 2 shows that the HAZ at the AS is smaller compared to that of the RS. Matching this hardness profile with the macrostructure in Fig. 1 indicates that the HAZ of the AS is the softest zone of the weld joint.

3. Experimental procedures

3.1. Indentation test procedure

The indentation experiments have been performed using the Zwick testing machine ZHU0.2/Z2.5, which is equipped with a hardness measuring head and a fully automated X/Y-table [20]. The built-in load cell measures electromechanically applied forces between 2 N and 200 N with the force resolution of 0.01 N and displacement measuring resolution of 0.02 μm. Integrated in the hardness measurement head are a digital travel measurement system on a glass scale with a resolution of 0.04 μm, a load cell and an interchangeable indenter. A diamond Rockwell indenter with a spherical tip radius of $R = 200$ μm was installed and used for all indentation tests. In the data analysis the residual stiffness of the testing equipment was set to be $C = 1 \times 10^6$ mN/μm. All experiments were performed under load-controlled condition in an air-conditioned room at a temperature of 21 °C.

The indentation tests were done with the multi-creep loading history consisting of three creep segments at $0.25P_0$, $0.5P_0$ and $0.75P_0$ of 100 s duration and a final creep segment at maximum load P_0 of $T_4 = 600$ s [21]. Another additional reloading-unloading process with $1.25P_0$ of 2 s duration is executed to complete the hysteresis loop of the 4th cycle. The maximum load P_0 has to be set to achieve the indentation depth h_0 in the range of 8–12% of the nominal indenter radius of $R = 200$ μm. For all indentation tests performed in this investigation, the maximum load, P_0, was set to 20 N

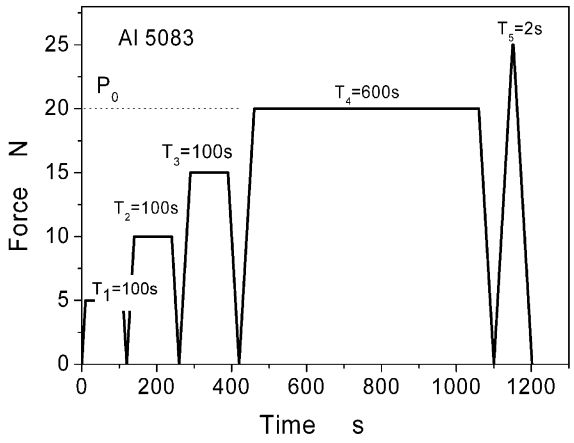

Fig. 3. Force–time function as used for all the indentation tests.

and the loading rate was 0.5 N/s as illustrated by the load history in Fig. 3.

3.1.1. Neural network analysis method

The method for analysing indentation curves via neural networks is based on a viscoplasticity model, which decomposes the total stress into a rate independent equilibrium stress Σ_E and the rate dependent overstress Σ_F. Their sum is the total stress for a given plastic strain and plastic strain rate. For small deformation theory and monotonic tensile loading the model can be simply written as [11]:

$$\sigma(\varepsilon_p, \dot{\varepsilon}_p) = \Sigma_E(\varepsilon_p) + \Sigma_F(\dot{\varepsilon}_p) = k_0 + \frac{\gamma}{\beta}(1 - e^{-\beta\varepsilon_p}) + \frac{3}{2}\frac{c}{b}(1 - e^{-b\varepsilon_p}) + (\eta\dot{\varepsilon}_p)^{1/m} \quad (1)$$

As written in Eq. (1), the equilibrium stress can be decomposed into its contributions, which are the isotropic and the kinematic hardening, each determined by two material parameters γ, β and c,b. The yield stress k_0 is given by the value of the isotropic hardening at zero plastic strain. When we assume that the hardening is purely isotropic, data from unloading-reloading hysteresis are ignored and (1) is reduced to:

$$\sigma(\varepsilon_p, \dot{\varepsilon}_p) = k_0 + \frac{\gamma}{\beta}(1 - e^{-\beta\varepsilon_p}) + (\eta\dot{\varepsilon}_p)^{1/m}. \quad (2)$$

The viscosity exponent m and the viscosity parameter η define the rate-dependent amount of overstress Σ_F. The maximum equilibrium stress is given by $\Sigma = k_0 + \gamma/\beta$, where the γ/β-ratio defines the maximum amount of work hardening during plastic deformation.

Using the well trained artificial neural networks, described in detail in [11,12], the material parameters in Eq. (1) or (2) and hence, the stress–strain behaviour of a material can be identified. The trained artificial neural networks are implemented in the PC application software "Indent Analyser", commercially available at ASMEC [13].

3.2. Indentation specimen preparation

A successful determination of local stress–strain curves via the NN-Method requires a high quality experimental determination of the force–depth curves. Frequently observed errors are associated with the preparation of the test specimen [22]. In cases where a standardized Rockwell indenter with a tip radius of $R = 200\,\mu m$ is used for the indentation tests, the maximum indentation depth at the end of the tests has to be within the range from 16 μm to 24 μm. This means that roughness of the indentation surface or possible cold work hardening in the test specimen surface layer due to milling, drilling or other mechanical treatments can significantly affect and spoil the force–depth curve. An often observed error source is unexpected test specimen movement due to an insufficient fixing of the specimen during the indentation test. Therefore, associated with the preparation of test specimen the user has to be aware of several factors which can bias the measured force and depth data.

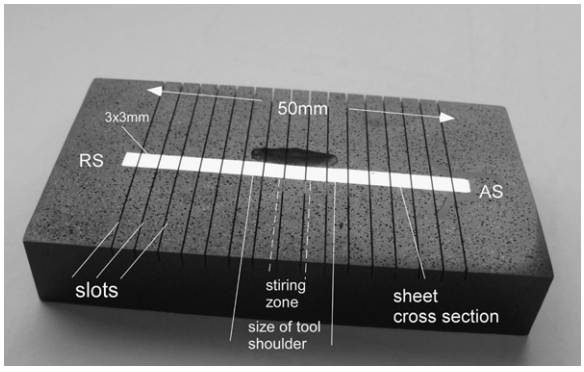

Fig. 4. Indentation test specimen imbedded in synthetic resin. The indentation surface was slotted in order to reduce possible in-plane residual stresses.

To enable high quality indentation tests, rectangular sections have been extracted from the weld seam. The sections were then imbedded into thermosetting synthetic resin. The top and bottom side of the resin block were then milled and grained to provide even surfaces. Finally the top side (indentation-surface) of the block was mechanically polished with abrasive paper from 320-grit down to 2400-grit following by diamond polishing with abrasive grit size of 3 μm and finalized with polishing SiO_2-solution. After this procedure the specimen surface on the top side of the block showed mirror quality associated with a surface roughness of $R_a = 0.2\,\mu m$.

Although it has not been measurements in this investigation, the weld joint carries presumably some residual stresses. In order to enable indentation tests on residual stress free material a further specimen was prepared as outlined above and then its surface was slotted by using a fine diamond saw blade. Fig. 4 shows the pattern of slots which have a depth and distance of 3 mm.

In order to verify how slotting is affecting the force–depth curve finite element simulations have been performed for the soft aluminium alloy AA 5083 and a high strength alloy AA 2024 T358 by using the axisymmetric FE-model presented by the insert given in

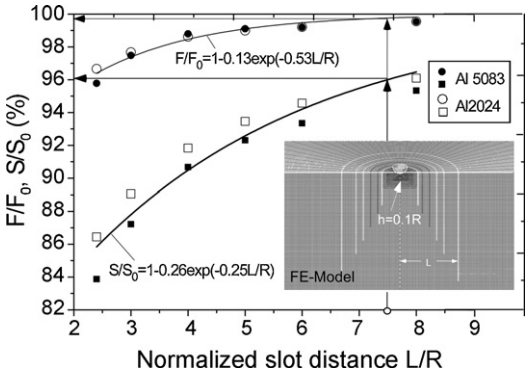

Fig. 5. Influence of column size, L, on indentation force, F, and unloading stiffness, S, at a fixed indentation depth of $h/R = 0.1$ obtained by finite element simulations on two materials using an axisymmetric 2D FE-model visualised as swept model. The individual lines in the FE-Model are slots which form 6 columns of different size. Arrows are marking the tests condition associated with the slotted test specimen used in the present investigation.

Table 1
Material input for finite element simulations of two different materials.

AA 2024 T351				AA 5083	
E = 70 GPa, ν = 0.3				E = 70 GPa, ν = 0.3	
log. plast. strain	True stress, MPa	log. plast. strain	True stress	log. plast. strain	True stress, MPa
0	343	0.295	630	0	200
0.0051	370	0.495	700	0.0050	251
0.0151	400	0.605	730	0.0154	277
0.0251	421	0.795	750	0.0270	299
0.0351	440	0.995	790	0.0351	310
0.0451	460			0.0453	323
0.0551	473			0.0555	335
0.0651	490			0.065	344
0.0751	498			0.075	354
0.0951	530			0.095	367
0.135	560			0.104	373
0.155	575			0.150	395
0.195	595			0.204	410

Fig. 5. It is a 2D finite element model visualised as swept model. The individual lines in the model are slots which form 6 columns of different size with a radius of L and depths of $2L$. A rigid contact surface was used to model the spherical indenter, which is displaced by maximum $h = 0.1R$ into the specimen surface. All nodes on planes $x = 0$, and $y = 0$ are fixed in these respective directions to model the symmetry conditions. The simulations are performed using ABAQUS. For each of the two materials finite element calculations have been performed for 6 different column sizes. For simulating the slots the Young's modulus of the selected slot elements displayed by the lines in the FE-model have been set to a very small value of 1 GPa. For both materials the multilinear stress–strain input data used for the finite element calculations are listed in Table 1.

Note, the simplification of the FE-model from slotted cubes with a side length $2L$ to a column with a diameter and depth of $2L$ is conservative with regard to a possible constraint effect on indentation force and unloading stiffness.

For both alloys the results of the finite element simulations are summarized by the data points in Fig. 5. It displays the influence of the column size to indenter radius ratio L/R on both the indentation force, F, and the unloading stiffness, S, at a fixed indentation depth of $h = 0.1R$. The ratios F/F_0 and S/S_0 represent the percentages of remaining force and remaining unloading stiffness of a slotted specimen with respect to a non-slotted specimen. With increasing L/R the influence of the free boundary on the indentation force F and unloading stiffness S diminishes gradually. As a first approximation it can be assumed that the effect decreases exponentially with increasing slot distance L/R. By fitting the finite element results, fit functions of the form $F/F_0 = 1 - 0.094\exp(-0.45L/R)$ and $S/S_0 = 1 - 0.237\exp(-0.25L/R)$ have been obtained for the force and unloading stiffness reduction, respectively. From Fig. 5 it can also be seen that the stiffness reduction and force reduction is similar for both materials and hence, it is not much affected by its difference in strength. The test specimen used in the present work has a slot distance of $2L = 3$ mm and the applied indenter tip radius is $R = 0.2$ mm which yields an L/R ration 7.5. For this test condition the finite element results in Fig. 5 provide a force reduction and unloading stiffness reduction by less than 0.5% and 4%, respectively. For most engineering applications this small effect is negligible. Hence, for the present work it may be assumed that force–depths curves measured on the slotted specimens are representing the mechanical property of a residual stress free test material.

3.2.1. Micro-tensile tests

Flat micro-tensile specimens have been machined by using electrical spark erosion technique. The weld joint was cut in thin slices as illustrated in Fig. 6. About 50 micro-tensile specimens were machined across the welded joint sampling the BM, HAZ, TMAZ and the stir zone. The thickness of the specimen was about 0.4 mm. The mid-section of the specimens was 10 mm in length and 1.4 mm in width. During the tensile test the elongation of the specimen was measured within the mid section of the specimen via an initial gauge length, $l_o = 8$ mm by using a laser extensometer (Fiedler P50). A special specimen fixture was used to assure uniaxial and bending-free loading condition. All tests were done using a constant grip-displacement rate of 0.2 mm/min.

4. Results and discussion

4.1. Results of indentation tests

For investigating the deformation properties of the weld joint one as-welded (i.e. non-slotted) specimen and one slotted speci-

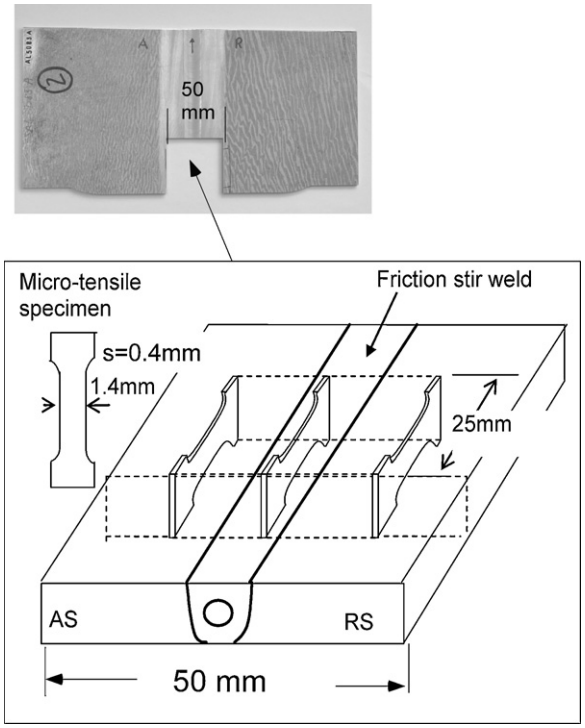

Fig. 6. Micro-tensile specimens machined from the FSW-weld joint by electrical discharging technique.

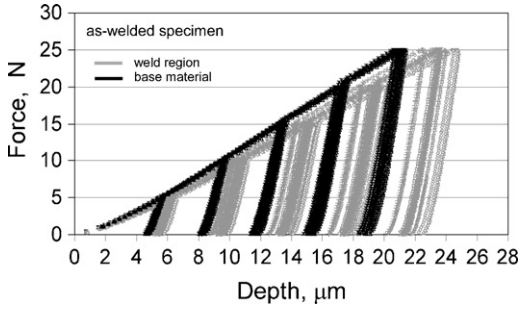

Fig. 7. About 30 force–depth curves measured across the weld joint of the as-welded indentation specimen.

mens have been tested. In case of the non-slotted specimen about 30 indentation tests with a distance of 1 mm were performed along the path across the weld joint. Mechanical slotting of the specimen produces an array of small squares on the specimen surface, which have a lateral length of 3 mm, see Fig. 4. For this type of specimen 12 indentation tests with a distance of about 3 mm were done across the joint. As shown in Fig. 2, a significant hardness drop is observed at distances closer than 7 mm to the weld joint centreline. This soft region covers the HAZs, the TMAZs and the stir zone. At distances larger than 7 mm the hardness values of base material is obtained. As an example Fig. 7 presents all the force–depth curves obtained from the as-welded specimen. In agreement with the trend observed for hardness data, the indentation curves have been separated into two distinct groups. One group of curves have been measured within the "weld region" that is at distances smaller than 7 mm to the weld joint centreline whereas the remaining curves have been measure outside the weld region designated as "base material". The force–depth curves derived from the slotted specimen are not explicitly shown here because they fall within the scatter band seen in Fig. 7.

In order to identify the material parameters of the various microstructures all indentation curves have been analysed using "Indent Analyser, Version 2.1.0". Besides the determination of the isotropic hardening parameters, the software also provides an option aimed at the identification of possible kinematic hardening parameters. Within that option the software is analysing the hysteresis loop of the force–depth curve as it is generated by unloading and reloading of the indenter during the indentation test. Because the AA 5083 material showed very small hysteresis loops this option was not applied in the present investigation. Hence, all measured force–depth curves have been analysed according to Eq. (2), which assumes that the stress in the material is composed by a linear elastic part followed by a non-linear isotropic hardening contribution and a strain-rate dependent overstress. Therefore, this analysis option identifies the yield strength k_0, the isotropic hardening parameters β, γ and the viscosity parameters m, η from each individual force–depth curve.

The approach allows to quantity material parameter variation across the weld joint. Generally it was found that all the identified parameters showed considerable scatter across the welded joint. Although it has not been explicitly investigated in this paper, there are a number of reasons which may have cause the scatter for example local changes of the microstructure, uncertainties of the neutral network parameter identification or experimental uncertainties associated with the indentation test itself. Investigating the behaviour of the individual material parameters k_0, γ, β, η, m only the yield strength k_0 and the parameter β showed a significant trend across the weld joint. The yield strength k_0 tends to be lower in the "weld region" compared to that in "base material", see Fig. 8a. This trend is consistent with the hardness results shown in Fig. 2. In case of the β parameter it more meaningful to examine

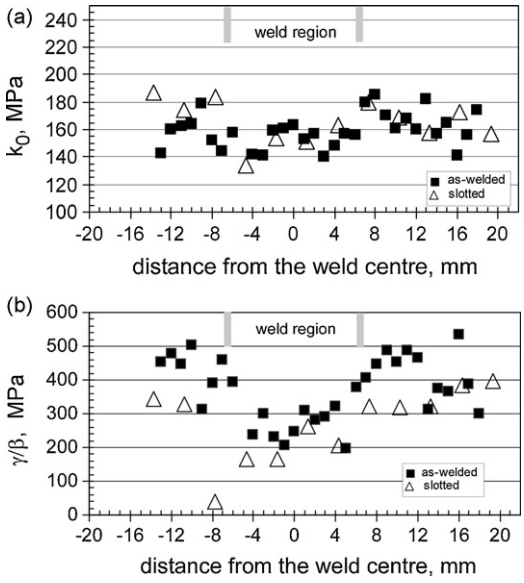

Fig. 8. Identified material parameters across the weld joint (a) yield strength, k_0; (b) maximum strain hardening capacity, γ/β.

the behaviour of the γ/β ratio because it quantifies the maximum work hardening during plastic deformation. As shown in Fig. 8b the material located in the "weld regime" has a smaller maximum work hardening than that of "base material".

Comparing the individual material parameters obtained from slotted specimens with that obtained from as-welded specimen it is generally observed that both fall in the same scatter band. An example is given by Fig. 8a which shows very good agreement between the k_0 values obtained from the slotted and as-welded specimen. Other investigations have demonstrated that k_0 is very sensitive concerning changes of residual stress [22]. Therefore, the fact that k_0 values from slotted and as-welded specimens are very similar promotes the assumption that both types of specimens (slotted and as-welded) are not containing a significant amount of residual stress. This would mean that the derived force–depth curves and hence, the corresponding identified material property parameters derived from the two types of specimens are presenting that of residual stress free bulk material.

4.2. Local stress–strain curves of indentation tests and micro-tensile tests

Local stress–strain curves of micro-tensile tests are used in the fields of weld joint qualification or as input for numerical simulations aimed at safety assessment of welded structures [23,24]. To introduce indentation testing as an efficient technique, it is of practical interest to compare the stress–strain curves obtained by indentation test with that of micro-tensile tests.

The different types of stress–strain curves obtained in this investigation are presented in Fig. 9a–c. Associated with the hardness results the stress–strain curves have been separated in two groups. One group contains stress–strain curves obtained from the "weld region" that is material located closer than 7 mm to the weld joint centreline. The second group of stress–strain curves characterizes material located outside that region designated as "base material".

The stress–strain data in Fig. 9a were calculated by converting engineering stress and engineering strain into true stress and logarithmic strain by the following equation

$$\sigma_{\text{true}} = \sigma_{\text{eng}}(1 + \varepsilon_{\text{eng}}); \qquad \varepsilon_{\log} = \ln(1 + \varepsilon_{\text{eng}}) \tag{3}$$

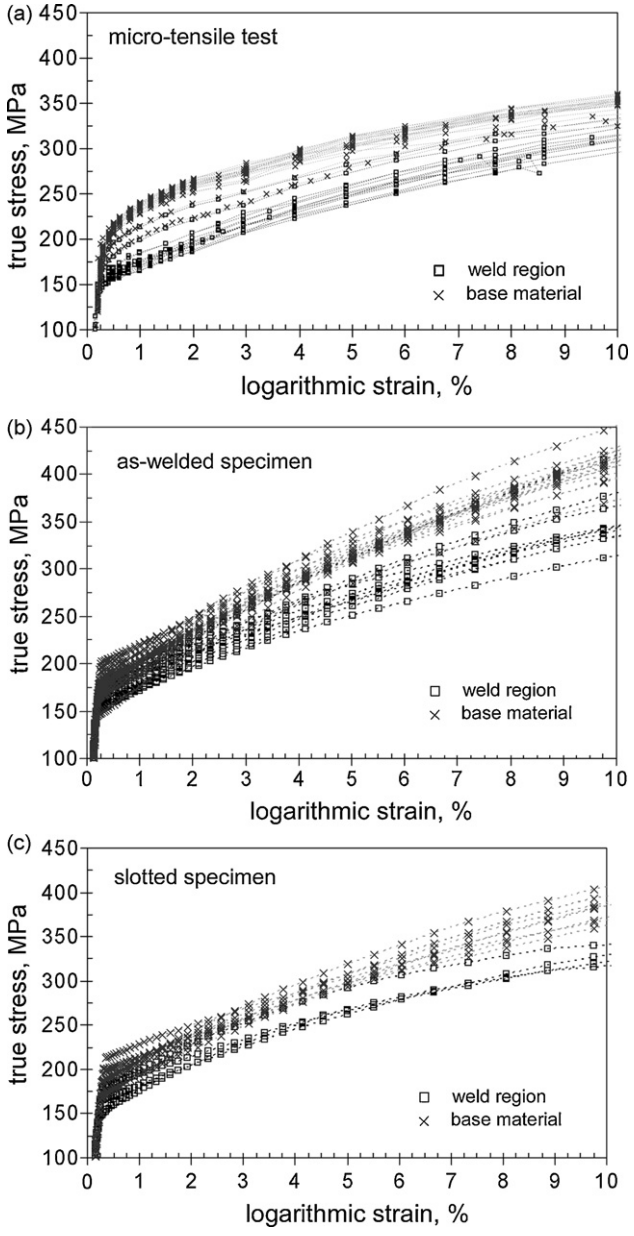

Fig. 9. Local stress–strain curves across the FSW-joint as derived by (a) micro-specimen testing, (b) indentation tests on as-welded specimen, (c) indentation tests on slotted specimen.

Eq. (3) becomes invalid when necking of the micro-tensile specimen is starting during the tests. Therefore, the ends of the individual stress–strain curves displayed in Fig. 9a coincide with a start of specimen-necking rather than with final fracture of the small tensile specimens. In general it was observed that necking of weld material starts at lower strains compared to that of base material. For this reason the number of weld material stress–strain curves in Fig. 9a becomes reduced at strains larger than 8%. In contrast to this limitation, the nature of indentation tests excludes specimen-necking and specimen-fracture. Therefore, the indentation tests always provide stress–strain curves over the entire strain region displayed in Fig. 9.

As previously stated, for practical application purpose it is of particular interest to study possible differences between of the three types of stress–strain curves presented by Fig. 9a–c. For comparison purpose it has to be taken into account that the total number of stress–strain curves in each diagram of Fig. 9 is quite different. Fig. 9a shows nearly 50 curves derived by micro-tensile tests, Fig. 9b has about 30 curves determined by indentation tests on as-welded specimen. Due to slotting of the indentation specimen Fig. 9c provides only 12 curves in total and just 4 curves could be derived inside the heterogeneous weld region. Hence, a simple comparison of the scatter bands displayed in Fig. 9 or a comparison based on average-value stress–strain curves is not very meaningful regarding the characterisation of local material property variations across the weld. A more meaningful comparison of the different types of stress–strain curves is obtained by converting the stress–strain curves of Fig. 9 into the four diagrams shown by Fig. 10a–d which are displaying true stress-data across the weld joint associated with constant logarithmic strain-values of 1%, 2%, 4% and 8%.

For a proper interpretation of the stress–strain curves it is important to consider that the applied strain rates used for indentation tests and micro-tensile tests are different. In such case the stress–strain curves as obtained from both types of tests contain different amount of overstress. This leads to the situation that even in cases where identical material is considered both tests methods may provide different stress–strain curves due to different amount of overstress.

As demonstrated by the material model (see Eqs. (1) and (2)) the overstress is calculated by $\Sigma_F = (\eta\dot{\varepsilon}_p)^{1/m}$ where $\dot{\varepsilon}_p$ is the plastic strain rate as applied in the test. For micro-tensile test and indentation test, the strain rate and hence, the overstress can be easily assessed by using some simplified considerations as follows: The micro-tensile specimens have been tested using a displacement rate of $\dot{v} = 0.2$ mm/ min which is picked up over a specimen length of $l = 10$ mm. Under such test condition the strain rate is approximately $\dot{\varepsilon} = \dot{v}/l = 0.0003/\text{s}$.

In case of ball indentation a representative strain can be calculated by $\varepsilon_r = 0.2a/R$ where R is the indenter radius, a is the indentation contact radius to be estimated by $a = \sqrt{2Rh - h^2}$ where h is the indentation depth [25]. In the present indentation test a Rockwell indenter with a tip radius of $R = 0.2$ mm is pushed into the specimen surface with a constant loading rate of $\dot{F} = 0.5$ N/s. All tests are terminated by a maximum force of $F_{max} = 25$ N which is associated with a maximum depth of approximately $h_{max} = 20$ μm. At this point the representative strain calculation yields a maximum strain of about $\varepsilon_{max} \approx 0.09$. For simplification it is assumed that the force–depth curves in Fig. 7 are linear. This means that the maximum force of 25 N and the corresponding maximum strain of 9% is reached in 50 s which determines a strain rate of approximately $\dot{\varepsilon} = 0.0018/\text{s}$.

Fig. 11 is showing the amount of overstress for two distinct strain rates of 0.0003 s^{-1} and 0.0015 s^{-1}, which are closed to that applied for the indentation tests and micro-tensile tests. The overstress in Fig. 11 was calculated by the equation $\Sigma_F = (\eta\dot{\varepsilon}_p)^{1/m}$ where the individual m- and η-values as identified across the weld joint have been adopted for these calculations. It can be seen that the overstress difference between the two different strain rates is just as small as 5 MPa. Such small overstress difference is only marginal affecting the stress–strain curves. Hence, the deviations between stress-data of indentation tests and micro-tensile tests as seen in Fig. 10 are mainly caused by other reasons than an overstress effect.

Comparing the diagrams in Fig. 10 several trends can be discovered. In all four diagrams of Fig. 10 it appears that the stress-data derived from the indentation tests show more scatter than those derived from micro-tensile tests. As already mentioned in conjunction with the observed scatter of material parameter, the scatter of the stress-data may have multiple reasons such as local changes of the microstructure, uncertainties within the neutral network analysis and experimental scatter associated with application of the tests procedure. A further point may be that an indentation

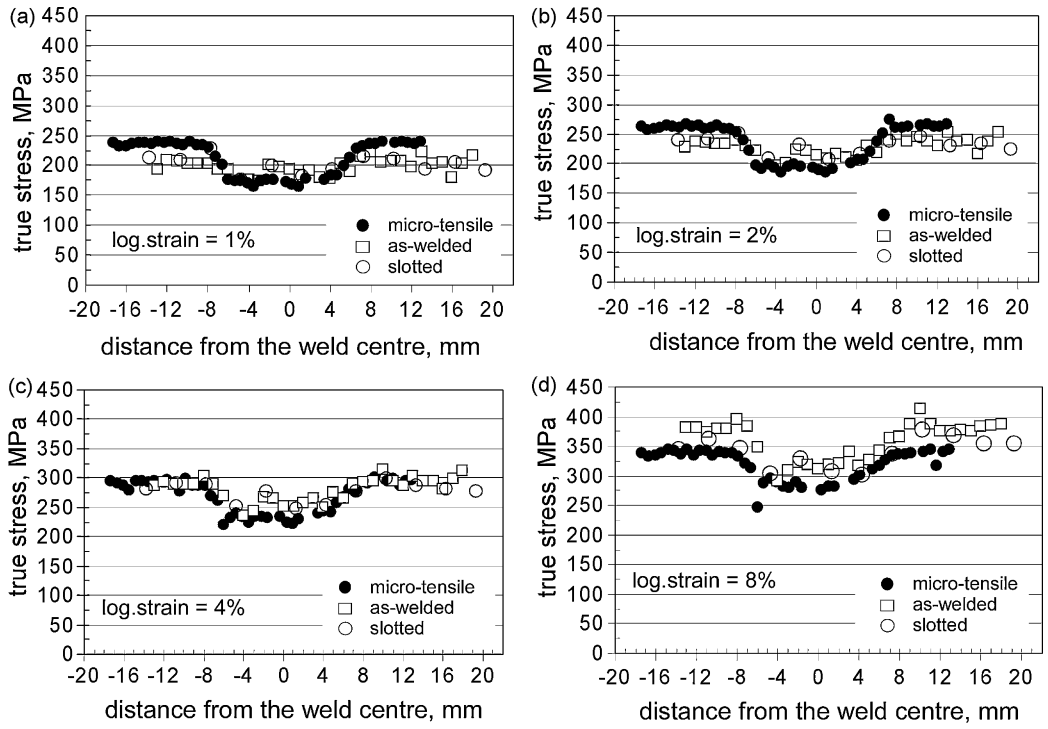

Fig. 10. Tue stress values across the weld joint associated with constant logarithmic strains of (a) 1%, (b) 2%, (c) 4%, and (d) 8% as obtained by micro-tensile tests and indentation tests.

test performed with a small indenter is sampling a much smaller material volume compared to that of a single micro-tensile test. Therefore, such indentation test will be more sensitive concerning the registration of local material property variation compared to a micro-specimen tensile test. Hence, more scatter is expected for the indentation test results.

The four diagrams of Fig. 10 can also be used to study how strain is affecting the stress-data obtained by the different test methods. Comparing the stress-data of micro-tensile test with that of indentation tests at four different strains of 1%, 2%, 4% and 8% it can be seen that with increasing strain, the stress-data located within the "weld region" and stress-data located in "base material" show a different trend. In the weld region the stress-data obtained from the indentation tests are always slightly overestimating the stress-data of micro-tensile tests by about 10%. Such overestimation is also observed for $R_{p0.2}$-values of "weld material", see Fig. 12. Analysing the behaviour of stress-data obtained in "base material" it appears that at small strains the stress-data derived from indentation tests are underestimating that of micro-tensile tests. At small strains of 0.2% the $R_{p0.2}$-values of base material obtained from indentation tests are about 12% lower than that of micro-tensile tests, see Fig. 12. With increasing strain this underestimation reduces continuously and at 8% strain the stress-data of indentation tests are overestimating that of micro-tensile tests by about 12%, see Fig. 10d. Comparing the stress-data obtained from slotted and as-welded specimens in Fig. 10a–d no significant difference between the two specimen types is observed. Therefore, the trends outlined in the former section are valid for tests on slotted and as-welded specimens.

Analysing the elastic slopes of stress–strain curves of micro-tensile tests reveals elastic moduli which scatter within the range from $E = 60$ GPa to 83 GPa. To our experience such scatter is typical for micro-tensile specimen tests. It is mainly caused by uncertainties associated with the specimen elongation measurements via the laser scanner technique. The "Indent Analysis" software was also used to identify elastic moduli from each force–depth curves. The identified E-values in Fig. 13 are close to that obtained by micro-tensile tests but there seems to be a difference between the E-values of slotted and as-welded specimens. Practical experience with the indentation method has shown that differences of identified E-

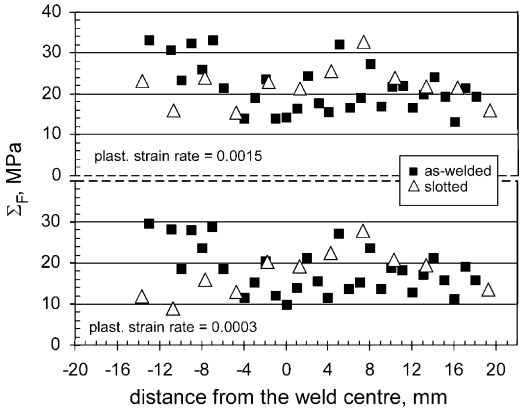

Fig. 11. Rate dependent amount of overstress across the weld joint calculated for two distinct strain rates of 0.0015 s^{-1} and 0.0003 s^{-1}.

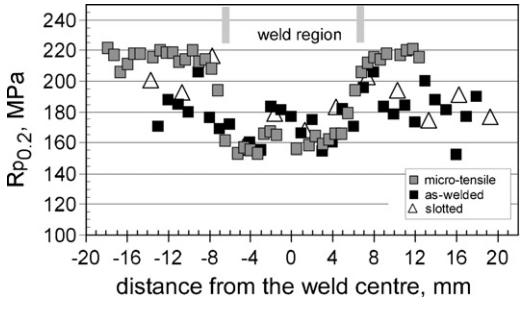

Fig. 12. $R_{p0.2}$ yield stress across the weld joint derived by indentation testing and by micro-tensile testing.

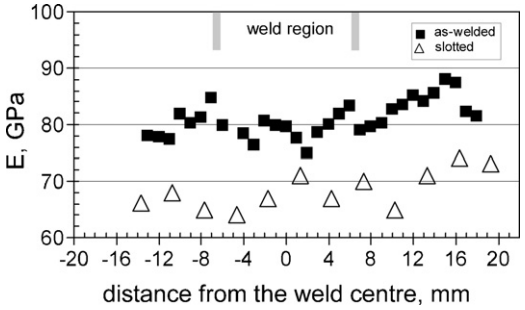

Fig. 13. Elastic-modulus across the weld joint derived by indentation testing.

values as is it seen in Fig. 13 are often caused by a change of the indentation tests specimen stiffness. The finite element simulation in Fig. 5 is predicting a 4% stiffness reduction due the slotting of the tests specimen. This effect may contribute to the disagreement seen in Fig. 13.

From the calculations and observation in the previous section it appears that the amount of rate dependent overstress is similar for indentation tests and micro-tensile tests. Therefore, overstress does not significantly contribute the observed differences between stress–strain curves. Moreover, the fact that k_0 values obtained from slotted and as-welded specimens are very similar promotes the assumption that both types of indentation specimens do not carry a significant amount of residual stress. Hence, the identified material parameters and resulting stress–strain curves are probably not significantly spoiled by a residual stress effect. Regarding possible residual stress in micro-tensile specimen, it is also reasonable to assume that micro-tensile specimens do not carry a significant amount of residual stresses by the following reasons. The specimens have been machined by using the spark erosion technique. This technique avoids work hardening of the specimen surface layer. In addition, associated with machining of the specimens, the weld joint was cut in pieces as small as the micro-tensile specimen. Such cutting is reducing residual stresses which may have been present in the original weld joint. Therefore, according to theses considerations it is not plausible that the observed differences between stress–strain curve of indentation tests and micro-tensile tests are caused by a residual stress effect. Certainly, the former assumptions concerning residual stress should be further justified by actual residual stress measurements which have not been performed in the present investigation.

It is worth noting that the observed trends and differences between the stress-data of indentation tests and micro-tensile tests are in agreement with recent theoretical investigations where the uncertainty of the stress–strain curve identification via the present neural networks has been investigated in detail [26]. As it is the nature of neural networks in general, also the neural networks as applied in the present investigation always provide an approximation of the "real stress–strain curve" of a material. In Ref. [26] it was found that the quality of the approximation depends on the stress–strain curve itself. Therefore, the quality of the parameter identification will differ from material to material. This may explain way stress–strain curves of weld material show a better agreement than stress–strain curves of base material as it is seen in the present investigation. Several practical applications of the method to base material have demonstrate that the identified stress–strain curve can deviate by about ±10% in stress from that of tensile tests [11,12,22,26]. This is about the deviation as observed in present investigations. Therefore, the results shown in this article indicate that indentation tests combined with neural network analysis is valid for characterising the complex stress–strain property variations in the present in FSW-joint. The investigations indicate further that the remaining difference between the stress–strain curves of micro-tensile tests and indentation tests are mainly caused by uncertainties of the neural network material parameter identification.

5. Summary

Instrumented indentation test combined with neural network analysis has been used to characterize complex mechanical property variations in AA 5083 friction stir weld joint. It was found that local stress–strain curves obtained from the indentation testing are compatible with that of conventional micro-tensile testing. Comparing the individual stress–strain curves of indentation tests with that obtained from micro-tensile tests it is found that the stress difference between the two types of stress–strain curves seems to be within the limits as it has been found in other investigations, which is about ±10% in stress. The findings in the present investigation indicate that such deviations are mainly cause by uncertainties associated with the neural network material parameter identification whereas strain rate effects and residual stress effects are only marginal contributing to the observed stress–strain curve deviations.

The present work demonstrates the validity of the instrumented indentation test method to provide local stress–strain curves as well as a number of material property parameters in complex AA 5083 friction stir weld joint with less experimental effort compared to the micro-tensile test method. The advantages of an easy and fast application of the indentation test method as well as the small required tests volumes offer a number of interesting applications in the field of mechanical weld joint characterisation. Other types of weld joints and metallic materials are presently under investigation in order to gain a broader knowledge about the applicability and validity of this indentation test method.

References

[1] A. Motarjemi, M. Kocak, V. Ventzke, Int. J. Pressure Vessel Piping 7 (2002) 181.
[2] S.T. Amancio, S. Sheikhi, J.F. dos Santos, C. Bolfarini, J. Mater. Process. Technol. 206 (1–3) (2008) 132.
[3] Ü. Ceyhan, Clausthal-Zellerfeld: Papierflieger, 2007, ISBN: 978-3-89720-882-7*Pb, http://www.gbv.de/dms/clausthal/E_DISS/2007/db108543.pdf.
[4] J.S. Field, M.V. Swain, J. Mater. Res. 10 (1995) 101.
[5] B. Taljat, T. Zacharia, Int. J. Solids Struct. 35 (33) (1998) 4411.
[6] S. Kucharski, Z. Mroz, Mater. Sci. Eng. 318 (1–2) (2001) 65.
[7] S. Kucharski, Z. Mroz, J. Eng. Mater. Technol.-Trans. ASME 123 (2004) 245.
[8] M. Zhao, N. Ogasawara, N. Chiba, X. Chen, Acta Mater. 54 (2006) 23.
[9] Y. Cao, X. Qian, N. Huber, Mater. Sci. Eng. A 454–455 (2007) 1.
[10] N. Huber, Ch. Tsakmakis, J. Mater. Res. 19 (1) (2004) 101.
[11] E. Tyulyukovskiy, N. Huber, J. Mater. Res. 21 (3) (2006) 664.
[12] D. Klötzer, Ch. Ullner, E. Tyulyukovskiy, N. Huber, J. Mater. Res. 21 (3) (2006) 677.
[13] ASMEC Advanced Surface Mechanics GmbH, Radeberg, Germany, http://www.asmec.de/software/IndentAnalyser-Help.pdf.
[14] E. Tyulyukovskiy, N. Huber, J. Mech. Phys. Solids 55 (2007) 391.
[15] N. Huber, E. Tyulyukovskiy, H.-C. Schneider, R. Rolli, M. Weick, J. Nucl. Mater. 377 (2008) 352.
[16] N. Huber, J. Heerens, Acta Mater. 56 (2008) 6205.
[17] H.N.B. Schmidt, T.L. Dickerson, J.H. Hattel, Acta Mater. 54 (2006) 1199.
[18] K.N. Krishnan, Mater. Sci. Eng. A 327 (2002) 246.
[19] Z.W. Chen, T. Pasang, Y. Qi, Mater. Sci. Eng. A 474 (2008) 312–316.
[20] Testing Machines and Systems for Metals (brochure), Available at: http://www.zwick.com/frame/Control.php?action=Frame,show&mainNavId=11.
[21] E. Tyulyukovskiy, Ph.D. Thesis, FZKA-Report 7103, March 2005, http://bibliothek.fzk.de/zb/berichte/FZKA7103.pdf.
[22] J. Heerens, F. Mubarok an, N. Huber, J. Mater. Res. 24 (3) (2009) 907.
[23] I. Scheider, W. Brocks, A. Cornec, Proc. Trans. ASME, J. Eng. Mater. Tech. 126 (2004).
[24] P. Cambresy, Report of GKSS Research Centre, GKSS 2006/5, 2006.
[25] D. Tabor, Cambridge University Press, 1951.
[26] S. Scherrer-Rudiy, Ph.D. Thesis, Fak. F. Maschinenbau, Uni. Karlsruhe, 2009, http://digbib.ubn.uni-karlsruhe.de/volltext/1000013646.